Elsevier Editorial System(tm) for Composites Part B

Manuscript Draft

Manuscript Number: JCOMB-D-16-00613

Title: Novel "load adaptive algorithm based" procedure for 3D printing of lattice-based components showing parametric curved micro-beams

Article Type: SI: COMPOSITE LATTICE

Keywords: B. Directional orientation; B. Microstructure; C. Finite element analysis (FEA); D. Mechanical testing; 3D printing.

Corresponding Author: Dr. Francesco Naddeo, Ph.D.

Corresponding Author's Institution: University of Salerno

First Author: Francesco Naddeo, Ph.D.

Order of Authors: Francesco Naddeo, Ph.D.; Nicola Cappetti, Master Degree; Alessandro Naddeo, Master Degree

Abstract: This work deals with the development, the application and the experimental validation of a procedure based on an original algorithm, running in a finite element environment replacing the continuous mass of any solid with a cancellous bone-inspired lattice structure showing curved beams oriented on the basis of the external forces, sharing with it border and boundary conditions. For the validation of the new lattice structure a cubic representative volume element, showing curved micro-beams, was chosen, implementing periodic boundary conditions. At the end, the algorithm created a .stl file to be printed by a 3D printer using an appropriate polymer. The numerical results were compared with experimental results obtained by compression tests. Experimental/numerical correlation confirmed the validity of the FEM "beam element - based" lattice structure that could be applied to different solid shapes.

Suggested Reviewers: Roberto Guglielmo Citarella Master's degree
Associate Professor, Department of Industrial Engineering, Department of Industrial Engineering, University of Salerno, Via Giovanni Paolo II, 132, 84084, Fisciano (SA), Italy
rcitarella@unisa.it

Rocco Furferi
Department of Industrial Engineering, University of Firenze, Via Santa Marta, 3
rocco.furferi@unifi.it

Ernesto Reverchon
Full Professor, Department of Industrial Engineering, University of Salerno, Via Giovanni Paolo II, 132, 84084 Fisciano, SA, Italy
ereverchon@unisa.it
Ernesto Reverchon has developed strong skills in design and production of porous structures showing at the same time different levels of porosity to be used in the contest of computer aided tissue engineering.

Giovanni Francesco Solitro Ph.D.
Research Associate, Department of Orthopaedics, University of Illinois at Chicago, 835 South Wolcott Avenue. Chicago, United States of America
solitrogf@hotmail.com
Giovanni Francesco Solitro has developed strong skills in the Biomechanics especially in the mechanical characterization of the bone tissue and in the parametric variational CAD modeling.

Alessandro Ruggiero
Associate Professor, Department of Industrial Engineering, University of Salerno, Via Giovanni Paolo II, 132, 84084 Fisciano, SA, Italy
ruggiero@unisa.it

Opposed Reviewers:

Dear Editor

The paper entitled "*Novel "load adaptive algorithm based" procedure for 3D printing of lattice-based components showing parametric curved micro-beams*" by Francesco Naddeo, Nicola Cappetti and Alessandro Naddeo is an original article. The manuscript, including related data, figures and tables, has not been previously published and is not under consideration elsewhere.

This study deals with the development, the practical application and the experimental validation of a procedure based on an original algorithm (filed patent) that runs in a finite element environment; it operates inside a three-dimensional virtual solid of any shape, withstanding any kind of boundary conditions for both imposed displacements and loads (in the field of the static structures) replacing the continuous mass of the solid with an appropriate lattice structure, having cylindrical beams that are suitably curved and oriented according to the internal stresses induced by the boundary conditions, the new structure and the old one sharing the border. The user, in order to optimize the structural behavior, can manage several input parameters like average minimum distance between convergence nodes, target porosity, target average number of beams converging in each convergence node, curvature of the beams and beams' mechanical properties. By introducing parametric curved beams, this algorithm becomes a powerful tool capable to design a new porous material able to show a wide range of mechanical properties' values in output while maintaining a constant value of porosity i.e., a constant amount of material.

A cubic representative volume element was appropriately designed and sized to conduct sensitivity analyzes in order to show the effect of changes in these parameters on the mechanical performances of the new porous material. The finite element results were compared with experimental results obtained by compression tests conducted on two polymeric 3D printed cubic specimen showing two different value of curvature characterizing the beams, the other input parameters being equal. The simulation results,

in terms of Young's modulus, confirmed the validity of the beam element - based structure that could be applied to different solid shapes and materials.

Possible applications could be the production of those porous materials for which it is required a set amount of material, a set external shape and at the same time heterogeneity of the mechanical properties at the micro and macro levels as for example in the field of the computational aided tissue engineering for production of scaffolds (bone-like structured foams) and in the field of ergonomics for production of highly structured foams.

I will be glad if you want to consider this paper for publication in "*COMPOSITES PART B: ENGINEERING: JCOMB" - SPECIAL ISSUE ON "COMPOSITE LATTICE MATERIALS AND STRUCTURES".*

Thank you for your consideration,

Sincerely

Francesco Naddeo

Novel "load adaptive algorithm based" procedure for 3D printing of lattice-based components showing parametric curved micro-beams

Francesco Naddeo[a], Nicola Cappetti[a], Alessandro Naddeo[a]

[a] Department of Industrial Engineering, University of Salerno, Via Giovanni Paolo II, 132, 84084 Fisciano (SA) Italy.

frnaddeo@unisa.it, ncappetti@unisa.it, anaddeo@unisa.it

Corresponding author: Francesco Naddeo; frnaddeo@unisa.it

Abstract

This work deals with the development, the application and the experimental validation of a procedure based on an original algorithm, running in a finite element environment replacing the continuous mass of any solid with a cancellous bone-inspired lattice structure showing curved beams oriented on the basis of the external forces, sharing with it border and boundary conditions. For the validation of the new lattice structure a cubic representative volume element, showing curved micro-beams, was chosen, implementing periodic boundary conditions. At the end, the algorithm created a .stl file to be printed by a 3D printer using an appropriate polymer. The numerical results were compared with experimental results obtained by compression tests. Experimental/numerical correlation confirmed the validity of the FEM "beam element – based" lattice structure that could be applied to different solid shapes.

Keywords

B. Directional orientation; B. Microstructure; C. Finite element analysis (FEA); D. Mechanical testing; 3D printing.

1. Introduction

In the past, researchers have always tried to create optimized structures for loads, with special attention given to the amount of material used in order to reduce costs and lighten the structures since the finite element method (FEM) was invented. Since 2000 [1] researchers have developed, improved, and applied finite element-based topology optimization which include a maturation of classical methods [2]. The most important types of topology optimization are: density-based methods, which include the popular Solid Isotropic Material with Penalization (SIMP) technique; hard-kill methods, including Evolutionary Structural Optimization (ESO);

boundary variation methods; biologically inspired methods. In the area of biologically inspired engineering, we can note how living beings have developed biological tissues characterized by such optimized structures. For example, trabecular bone architecture undergoes adaptive changes that were first studied by Wolff [3], who described the trajectorial theory of trabecular orientation. Several mathematical models have been proposed for bone remodelling and various criticisms have been made on Wolff's law [4] about the one-to-one correspondence between the stress trajectories of continuous bodies and the discontinuous structure of the bone. The proposed models usually assumed bone tissue final configuration as a function of boundary conditions and bone to be a continuous, linearly elastic material. Anisotropic continuum-based models were used by Fernandes et al [5], Garcia et al [6] and Jacobs et al [7], while orthotropic continuum-based models were used by Cowin [8] and Huiskes and Hollister [9]. Some authors [10 - 11] have proposed Hierarchical multi-scale bone models, in which the micro/nanometric structure was taken into account. Tsubota et al [12] used large-scale voxel finite element models (FEMs) for simulating the trabecular bone remodelling. Optimization techniques were proposed by both Luo and An [13] and Boyle and Kim [14] while Hambli et al [11] introduced a coupled finite element and neural network computation method. Currently, as a non-destructive method in the field of mechanical behaviour research, finite element analysis is increasingly used as a way to realize new structures generally used for composite materials or porous materials not only to understand the internal stress distribution and the mechanical behaviour of already existing structures but also to design new structure. In this case, FEM results become input parameters managed by highly complex algorithms that, by means of looping procedures, are able to optimize virtual structures respect to a particular mechanical aspect.

The aim of this work was to create a highly structured porous material biologically inspired through the three-dimensional printing which, in the same manner of biological tissues and, in the present case, of cancellous bone (on the base of Wolff's law), is able to adapt itself to external loading conditions, showing, at the same time, a lightweight structure with the possibility to parameterize the homogenized mechanical properties by simply varying the sensitive parameters that describe the geometry of the structure. In many fields of research on

the highly structured porous materials, the production is often bound to the use of particular materials, to respect a particular external geometrical shape and a particular porosity, i.e., a particular amount of material. By using the presented algorithm, once you set the material to be used (compatibly with the possibility of printing it) you can, for example, set the porosity at a certain level and have access to a wide range of mechanical properties by varying a few geometric parameters in input. These are much sought-after qualities in the field of Computer Aided Tissue Engineering (CATE) for the production of scaffolds. Scaffolding materials for bone regeneration, for example, should be osteocondùctive and favour the adhesion and migration on the scaffolds of the osteoprogenitor cells that subsequently differentiate and form the new bone; for this reason the geometry of the porous material has to mimic that of natural biological tissue (that is generally naturally optimized to withstand the loads to which it is subjected during its life cycle). Furthermore in the design of such structures you must take into account the boundary conditions characterizing the period they will spend in bioreactors in which they will be subject to different types of mechanical stimuli both static and dynamic. In a previous study Baldino et al [15] have demonstrated that the curvature of the nanofiber is the parameter that most influences the weakness/stiffness of this kinds of porous material. For this reason we have developed a procedure based on an original algorithm [16], running in a finite element environment, operating inside a three-dimensional solid of any shape, withstanding any kind of boundary conditions for both imposed displacements and loads (in the field of the static structures) replacing the continuous mass of the solid with an appropriate lattice structure, having cylindrical beams directed according to the internal stresses induced by the boundary conditions, sharing with it border and boundary conditions. In this work, we have used parametric curved micro-beams in order to control the weakness of the whole structure after the optimization carried on by orienting the beams according to the boundary conditions. A cubic representative volume element (RVE) was appropriately selected and sized to conduct sensitivity analyzes to show the effect of changes in input parameters on the mechanical performances of the new porous material. The finite element results were compared with experimental results obtained by compression tests conducted on polymeric 3D printed cubic specimens. The simulation results in terms of Young's modulus confirmed the validity of the

"beam element – based" lattice structure that could be applied to different solid shapes and materials.

2. Materials and Methods

2.1 Description of the algorithm

The authors created an algorithm running in Ansys FEM environment able to create a virtual beam network (beams of any length, of any type of section and aspect ratio) with beams connected to each other at the end points with internal fixed joints, inside a solid of any geometric shape. The network shares with the solid the borders and the boundary conditions. The algorithm remodels the beam network obtaining a structure having the beams mostly oriented along the principal stress directions recorded in the continuous mass. After appropriate sizing of the beams, the algorithm gives us a new structure able to efficiently withstand the same boundary conditions with a considerable lightening of the structure, and consequently a notable reduction in materials used. In this work, in order to have a direct control on the mechanical properties of the final structure, a parametric curvature has been introduced for each cylindrical beam on the bases of studies reported in a previous work [17].

The algorithm consists of a single source code and has been written in ANSYS Parametric Design Language (APDL); during the calculation, the algorithm performs the following steps (Figure 1):

1. Initially, it takes in input the three-dimensional CAD (Computer Aided Design) geometry of the solid taken in consideration;
2. It creates a random distribution of keypoints (keypoint cloud) that is sufficiently uniformly distributed, and that occupies the volume of the solid;
3. for each generated keypoint, it defines a spherical space of selection (SSS) in order to intercept a specified number of keypoints [17] and generates line segments joining the initial keypoint, with each keypoint belonging to its SSS;
4. It activates a routine that conveniently eliminates both overlaps and intersections among line segments;

5. It creates the mesh of beam elements in each line segment [17 - 18], obtaining a lattice structure occupying the volume of the solid that shows an isotropic mechanical behaviour;
6. It applies to the FEM model linear material properties characterizing the real material behaviour;
7. It applies boundary conditions to the solid that simulate the real conditions;
8. It calculates the elastic solution due to the boundary conditions defined in step 7;
9. In post-processing, it sorts, in an array, all the identification numbers of the created beams in an ascending manner according to an appropriate criterion based on the magnitude of the stresses to which each element is subjected during the FEM virtual test.
10. It activates an iterative routine that, according to the array created in step 9, eliminates the beams starting from the first component of the array. The iteration stops at a specified number of beams such that the number of connections for each convergence node is equal to the desired average number of beams (ANB) converging on each node; simultaneously it activates an *ad hoc* routine able to guarantee structural continuity;
11. It activates a routine that eliminates the so-called “dead ends”; i.e., the branches of the structure made of beams that, having only a single point of connection with the rest of the structure, will not work [19];
12. In order to reach the desired homogenized mechanical property of the final product, it activates a routine that introduces a parametric curvature to each beam and at the same time resize the beams (varying the cross section) to achieve the desired porosity (i.e., fraction of the volume of voids over the total volume of the inputted solid).
13. It generates in CAD environment the solid model of the new structure;
14. It generates the file .stl for the following rapid prototyping phase in order to obtain the physical model.

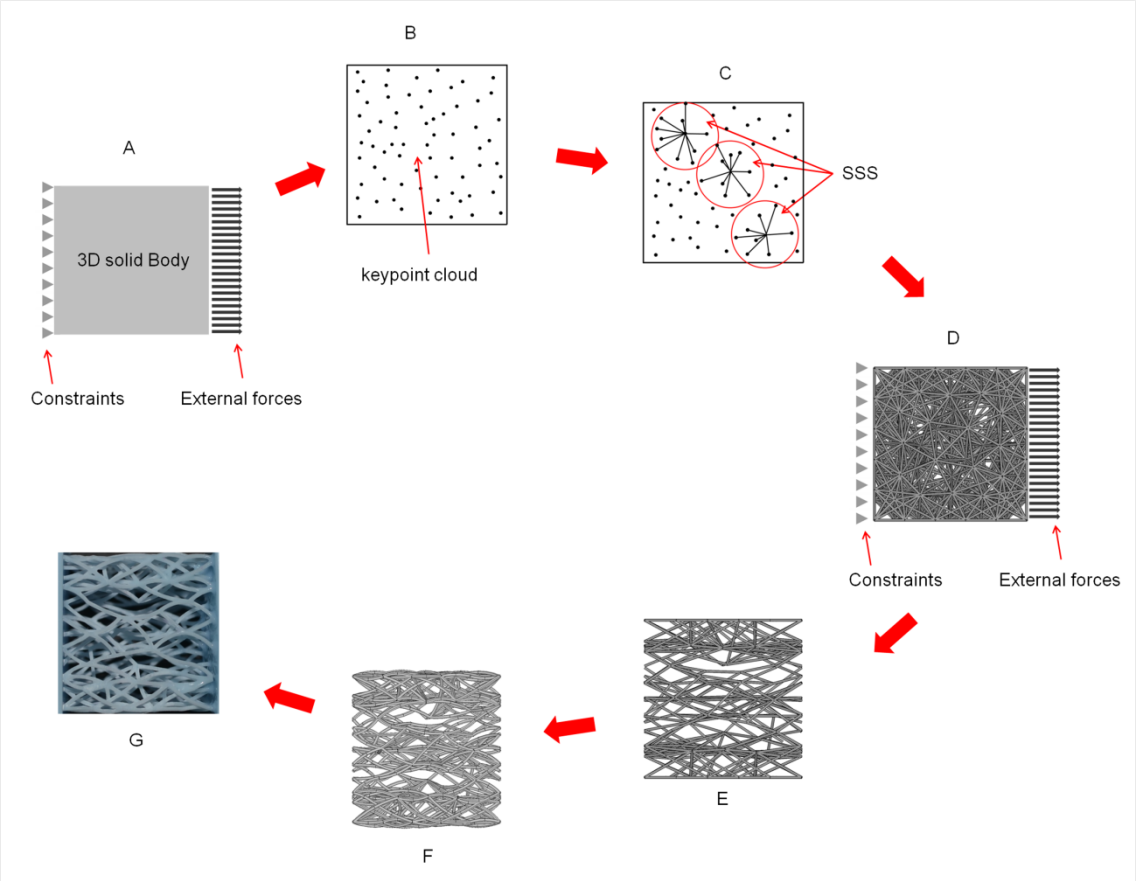

Figure 1. Algorithm fundamental steps for elaborating a generic cubic solid mass withstanding generic boundary conditions: A) step 1; B) step 2; C) steps 3 and 4; D) step 5 ; E) steps 6 - 11; F) steps 12 - 13; G) 3D printed polymeric specimen.

Previous studies [20] on the same topic, created three-dimensional beam-based structures by interpolating only the principal stress directions so that they did not select other elements that, being oriented not along isostatic lines may constitute real bracings and improve structural performance. In this work, the initial beam network (see step 5), that shows randomly oriented beams, allows for the most advantageous directions to be chosen to minimize the amount of material used, by eliminating selectively the less loaded beams until reaching a predefined number of converging beams for each convergence node. The final result consists of a new parametric curved beam network showing porosity set at a desired value, a desired ANB and that shares the border with the original solid. Beams are mostly oriented along the principal stress directions, whose convergence nodes have a desired average number of connections.

2.2 Input parameters

The algorithm's input parameters are the following:

- Average minimum distance between convergence nodes (*dist*) defined as a linear function of a characteristic size of the solid;
- Target porosity;
- Target ANB;
- Radius of the SSS, being a linear function of the previously defined "*dist*", that is chosen due to its appropriate ANB;
- Curvature of the beams;
- Mechanical properties.

2.3 FEM element type

In this work, we have implemented quadratic three-node straight beam elements in 3-D, showing circular cross section, which are suitable for analyzing slender to moderately stubby/thick beam structures. It takes account of both torsion-related shear stresses and flexure-related transverse-shear stresses, which henceforth will be generically referred to as "shear stresses" (τ), as the focus will be on their absolute maximum value and not on their causes. Six degrees of freedom occurred at each node for translations and rotations in directions *X*, *Y* and *Z*.

2.4 FEM mechanical properties

The first application of the algorithm consisted of the realization of a sensitivity analysis campaign on input parameters realized on an appropriate cubic RVE with the aim to evaluate the effects of changes in sensitive input parameters, specified in section 2.2, on the mechanical performance of the new material in linear elastic conditions. For this reason, for the mechanical characterization of the beams, the elastic modulus was set to E = 1 Pa while the Poisson's ratio was set to ν = 0.3 for ease of discussion and without any loss of generality. Later in the discussion, the chosen morphometric input data and the material properties of the polymer selected for printing and that have been introduced in the algorithm, will be reported.

2.5 RVE description and boundary conditions

In FEM analysis, the RVE should be large enough to contain all the intrinsic characteristics of the structure to be simulated, which, in our case, consists of geometrical characteristics and material properties. Cubic-shaped RVE (with a unitary volume for ease of discussion and without any loss of generality) was chosen to evaluate the mechanical performance of the algorithm; cubic-shaped RVE also allows an easy boundary conditioning.

The target of this work was to optimize the structure of the chosen RVE orienting first the beams according to the loads transmitted internally by the boundary conditions and, subsequently, introducing a variable curvature to the beams to calibrate, as needed, the value of the homogenized mechanical properties. In this study, the RVE was subjected to a virtual tensile test along the X axis parallel to one of the edges of the cubic RVE to allow the algorithm to properly orient the beams along this axis.

2.5.1 Periodic boundary conditions

All the simulations, which have been realized to create and size the FEM model, were carried out by applying PBC to the RVE allowing to calculate more accurately the elastic constants of the simulated material [21 - 22]. For the specific study of this cubic RVE, an *ad hoc* written FEM routine was used; this routine can automatically create an identical surface distribution of nodes for the opposite sides [23]. Further, these nodes are opportunely selected on the basis of their location since the conditions on the displacements, in this case, have to couple the displacements at each point located on opposite sides of the cubic RVE. These conditions can be expressed in the following synthetic matrix form:

$$u_2 - u_1 = \varepsilon(X_2 - X_1) \quad (1)$$

With ε, being the *strain tensor*, X_i (i = 1, 2) being the position vector of the points belonging to opposite sides of the RVE, and u_i being the relative displacement.

2.5.2 Homogenized modules

The routine described in 2.5.1, for each simulation can automatically perform three static tensile tests and three static shear tests (with imposed average strains) in order to have an exhaustive representation of the mechanical behaviour of the structure. Imposing the overall strain to the RVE: $\langle\varepsilon\rangle = [0 \dots \langle\varepsilon_i\rangle \dots 0]$, and assuming elastic behaviour and small strains of the material, for

each i-th imposed strain, the routine calculates all the components of the corresponding i-th column of the stiffness matrix using the following formulation (elastic overall constitutive law):

$$\overline{C_{hi}} = \frac{\langle \sigma_h \rangle}{\langle \varepsilon_i \rangle} \; \forall \text{ h, i = 1,...,6} \qquad (2)$$

with $\langle \sigma_h \rangle$ being the stress component calculated in the FEM post-processing environment, using the following relation:

$$\langle \sigma_h \rangle = \frac{\sum_{elem} \sigma_{h_{elem}} vol_{elem}}{vol_{RVE}} \qquad (3)$$

$\sigma_{h_{elem}}$ being the h-th stress component of the single FEM element, due to the i-th imposed strain, vol_{elem} being the element volume, and vol_{RVE} the volume of the RVE. In this way, the routine calculates all the components of the stiffness matrix with Eq. 2 by means of a single FEM run, characterized by six sequential imposed strains. Finally, the routine automatically provides the stiffness and compliance matrices of the examined cubic RVE in output.

2.5.3 RVE sizing

As reported previously, the main algorithm, in step 5 (see section 2.1), creates a beam network that tends to show isotropic material behaviour (see Figure 2). In terms of statistics, the increasing of the RVE size (i.e., increasing the number of beams) causes an increase in the material's isotropic degree. For this reason, intrinsic statistical characteristics were taken into consideration when choosing the RVE size in order to obtain an acceptable starting isotropic degree [22]. An original isotropic criterion [23 -15] to optimize the size of the cubic RVE was implemented. It is based on the minimization of the following function:

$$|\Delta|^2 = \sum_{i,j=1}^{6} \left(C_{i,j} - C_{i,j}^{I}(\lambda, G) \right)^2 \qquad (4)$$

with $C_{i,j}$ being the i, j-th component of the stiffness matrix, calculated from the FEM results; $C_{i,j}^{I}$ being the i, j-th component of the unknown isotropic stiffness matrix; and λ and G representing the independent parameters defining the isotropic stiffness matrix (Lamè constants). The minimization of Eq. 4 led to the determination of λ and G, i.e., the parameters defining the behaviour of the isotropic material closer to the behaviour of the material simulated by the FEM calculation. Consequently, an ad hoc written routine calculated the parameter *δ*, which was defined as the ratio of the norm of the "difference tensor" $\Delta = C - C^I$ to the norm of

the tensor C^I. The parameter δ provided information about the isotropic degree of the cubic RVE, which was directly related to the previously defined parameter "*dist*" of the RVE.

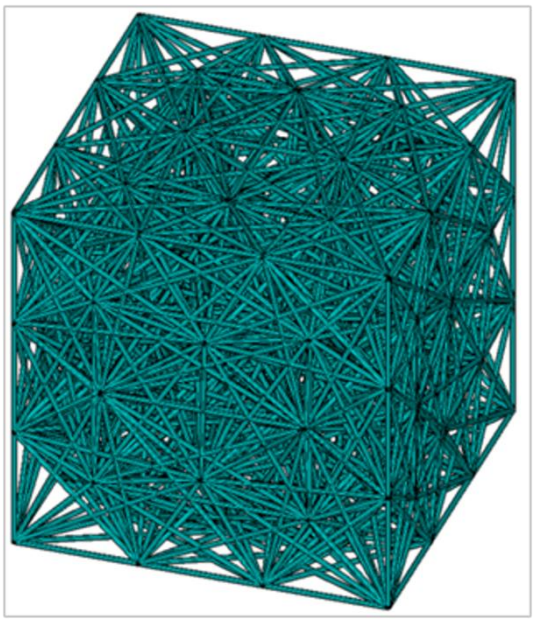

Figure 2. Example of an initial isotropic cubic RVE. For readability purposes, fewer mesh wires than those used in the calculation are represented.

The isotropic criterion showed that the value of the parameter δ tended towards a small constant value for $dist = \frac{Lrve}{10}$, with $Lrve$ being the edge length of the cubic RVE. In this way, the RVE size was not too large from a computational point of view, but sufficiently large to make the beams substantially oriented in a random manner. This structure gave to the RVE a sufficiently isotropic mechanical behaviour prior the application of the boundary conditions designed to orient the beams (see section 2.1, step 7).

2.6 Convergence analysis of the FEM results using straight beams

Increasing the number of elements for each beam did not cause an appreciable variation in the FEM results in terms of elastic moduli. For this reason, each beam was modelled by means of a single beam element [24, 25, 18].

2.7 Beam sorting criteria

In the post-processing environment (see section 2.1, step 10), the algorithm sorts, in an array, all the identification numbers of the created beams in an ascending order according to an appropriate criterion based on the magnitude of the stresses to which each element is subjected during the virtual test. The choice of the criterion can be based on considerations relating to both the real behaviour of the simulated material (material ductility and brittleness) and the boundary conditions. In the present study, three different output entities were considered for each beam element:

- The quantity of elastic strain energy stored during the calculation,

  $$\emptyset = \int C_{ijhk}\varepsilon_{ij}d\varepsilon_{hk} \quad (5)$$

  with C_{ijhk} being the generic component of the elastic tensor of fourth order, and ε_{ij} and ε_{hk}, the generic strain components;
- Maximum equivalent von Mises stress ($\sigma_{eq,\ Max\ (von\ Mises)}$);
- Maximum principal stress' absolute value ($\sigma_{principal,\ Max}$);

In the second criterion, a selection based on the amount of distortion energy stored by the beams during simulated tension/compression test (von Mises failure criterion for ductile material) is preferred. The third criterion, conversely, only considers the effect of the normal stresses stored in the beams (Coulomb and Mohr failure criteria for brittle materials). To achieve this, the main algorithm is equipped with specific routines designed to calculate/retrieve and sort the above variables for each element in the post-processing environment (see section 2.1, step 10).

2.8 introduction of curved beams

Once the RVE lattice structure was realized, the beams properly oriented and the porosity *P* set, the ratio of the average diameter to the length of the cylindrical beams is univocally determined. Some geometric aspects of the microstructure of porous materials can deeply affect their mechanical behaviour. For example aerogel is a very compliant material. Baldino et al [15] produced Poly-L-Lactid Acid aerogels for bone scaffolding whose nanometric structure was characterize by a network of curved fibres. In this work, it has been demonstrated, through a parametric FEM models, that the average curvature characterizing the fibres scaffolds, leads to a bending/buckling tendency, determining a higher weakness of the entire structure. This

observation was supported by a previous study by Ma et al [19] that, by means of modelling, tried to learn more about loop formation during the gel aggregation process and discovered that bending was the major mode of deformation of the network. Also Pirard and Pirard [26] proposed a mechanism based on the tendency of the network to buckle. In fact, in such lattice structure, the straight beams are basically subject to tensile-compression stresses (within small displacements), regardless of the type of boundary conditions applied to the nodes. It is possible to demonstrate that by substituting the straight beams with curved beams a bending moment appears for each beam, and that the bending moment contribution to the displacements becomes more prominent with increasing of curvature, especially if the ratio of the radius of curvature to beam thickness is greater than 10 as in the proposed FEM model [15]. These bending moments determine small local strains/stresses that, determine large deflections of the extremes of each beam; i.e., in case of equal displacements, the curved beam lattice structure will be subject to local strain/stress lower than the straight beam lattice structure. This phenomenon implies a low homogenized Young's modulus which results in a high softness of the whole structure. To advantage of this feature, we implemented a routine in the main algorithm that substitutes the straight beams of the lattice structure with parametric cylindrical curved beams based on spline curves (lying on a plane and having second order derivative at the endpoints equal to zero), modelling the cylinder axis, interpolating three points, two of which coincident with the endpoints of the beams and a third in a central position at a distance "*d*" from the straight segment linking the two endpoints; the plane of the spline curve being randomly oriented around the straight segment linking the two endpoints. The volume occupied by the beam network is:

$$V \cong \sum_{i=1}^{n} l_i(d)\Sigma \qquad (6)$$

n being the total number of beams, l_i the length of the i-th spline, which is a function of the parameter *d,* and Σ the cross section of the beams that does not vary with *i*. This routine produced an interpolating curve of output data points that describes the function $\frac{E_i}{E} = \varphi(d), \forall\, i \in [x, y, z]$, with *P* being constant, by using the relationship (6), E_i being the homogenized Young's modulus of the cubic RVE along the i-th axis and *E* being the input Young's modulus of the curved Beams. Figure 3 shows an example of the range of the homogenized Young's modulus

values to which it is possible to access by varying *d/dist*, once set *P* = 0.8, ANB = 6, SSS = 1.75.

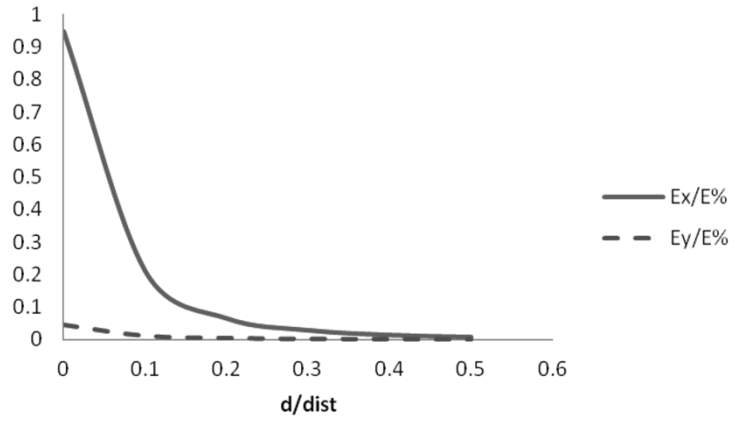

Figure 3. Percentage ratio of E_x *and* E_y to *E*, in function of the beams' curvature represented by "*d/dist*", the porosity *P* being constant; E_z has not been introduced in the graph since it is quite superimposable to E_y one.

If straight beams were implemented, once set the porosity, it could not be easily to vary the homogenized mechanical properties of the cubic RVE since the variation of the resistant section of the beams, for controlling these mechanical properties, would lead to a variation of the porosity. By introducing parametric curved beams this algorithm become a powerful tool capable to design a new porous material able to show a wide range of mechanical properties' values in output while maintaining a constant value of porosity i.e., a constant amount of material.

2.8.1 Convergence analysis of the FEM results using curved beams

A convergence analysis of the results (in terms of Young's Modulus) was performed choosing an average element size of the FEM model equal to *M* = *L*/12, *L* being the length of the curved beam, with a corresponding percentage error of 0.055 compared to the asymptotic value.

2.9. Sensitivity analysis campaign

A sensitivity analysis campaign was realized on an appropriate cubic RVE, after the orientation of the beams, with the aim to evaluate the effects of changes in sensitive input parameters, specified in paragraph 2.2, on the mechanical performance of the new material in linear elastic

behaviour range. We have used a simple “one factor at a time” approach, estimating the influence of some geometric parameters on the response by independently varying the parameters over a certain range. However, this approach is unable to clearly reveal possible interactions between parameters [27] but it gives us information about the potentiality in managing of such an algorithm.

2.9.1 Variation of the parameter SSS

The SSS size must ensure an initial ANB as to have available a fairly large number of orientations to be selected. An excessive large SSS size, however, determines computational errors caused by possible intersections between curved beams, difficult to model in CAD environment, with subsequent inability to create the .stl file for 3D printing. For this reason three values of SSS radius (1.5 x *dist*, 1.75 x *dist* and 2 x *dist*) were considered, the other input parameters being constant. The authors have judged the value of SSS radius equal to 1.75 x *dist* a fair compromise between fairly high value of the homogenized Young’s modulus and the risk of possible intersections between curved beams (if the curved beams remain, on average, of the same length, the probability that they intersect each other is greatly reduced). Furthermore, in this way there is a better accuracy in modelling the boundary of the solid when it presents curvatures with a radius of the same order of magnitude as the average minimum distance between the convergence nodes.

2.9.2 Variation of the parameter ANB

Subsequently, once set the SSS size, ANB was made to vary from a minimum of 3 to a maximum of 20. It was found that the homogenized Young’s modulus of the cubic RVE, in the loading direction (E_x), tends to decrease with increasing of ANB, while the other two Young's moduli (E_y and E_z) tend to increase, thus tending to the same value for ANB greater than 12. Thinking of a future production of bone scaffolds that have to mimic, among other things, also the geometric distribution of the trabeculae, ANB equal to 6 was chosen also taking account of the average number of converging trabeculae characterizing the transversely isotropic cancellous bone [18].

3. Three dimensional printing and mechanical tests

Two virtual models, characterized by the morphometric input data collected in the Table 1, were created using the algorithm described in this work that oriented the beams along the *X* axis. The aim was to print three-dimensional specimens to be tested in order to study the experimental/numerical correlation. The target of this phase of the study was to validate the FEM model characterized by a one-dimensional element (beams) based network. In this case, for ease of discussion and without any loss of generality, the parameters "*Lrve*" (length of the cubic RVE) and "*dist*" have been sized taking into account the characteristics of the 3D printer and of the available testing machine. The two models differ only in the curvature of the beams. The algorithm has provided, in output, two .iges files containing a set of solids representing the curved beams (inflected cylinders on the basis of spline generated by the algorithm) and the convergence nodes (spheres whose radius is equal to the inflected cylinders' radius).

Table 1 Morphometric input parameters characterizing the two cubic RVEs to be printed.

	RVE1	**RVE2**
Lrve	2cm	2cm
dist	Lrve/5	Lrve/5
SSS radius	dist*1.75	dist*1.75
Porosity	0.95	0.95
d/dist	0.1	0.25
ANB	4	4

These files have been treated with a special routine in CAD simulation environment to fuse the various solids together and create the .stl files to be supplied to the 3D printer. For printing we have chosen a 3D printer (DWS 020D produced by DWS srl - Via Lago di Levico, 3 - 36010 Zanè (VI) Italy); the specimens were equipped with rigid bases perpendicular to the axes of compression in such a way they also acted as a supporting material during the printing phase (see Figure 4). Compression mechanical properties of the printed material were measured using a CMT4000 Series (by SANS, China). The cubic specimens were compressed at a cross-head speed of 1mm/min along *X*, *Y* and *Z* directions. Five specimens were tested for each configuration.

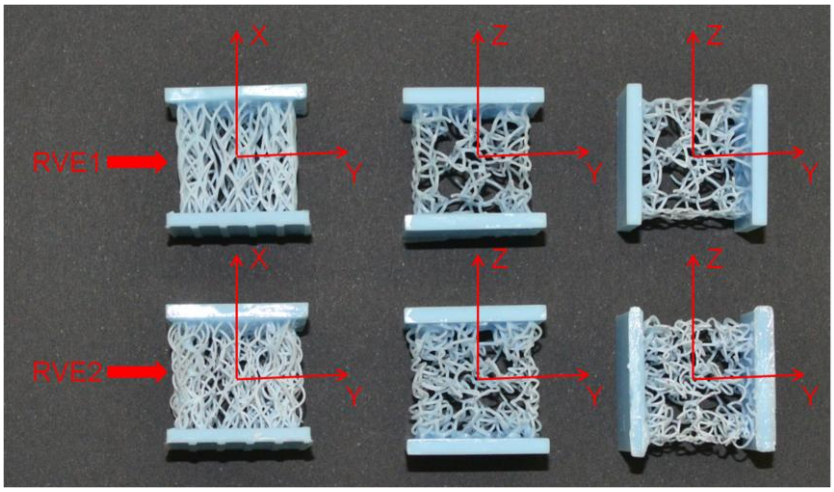

Figure 4. Printed specimens: in the first row, the three configurations of the RVE1 specimen are shown; in the second row, the three configurations of the RVE2 specimen are shown.

4. Experiments

The algorithm was optimized to process the cubic RVE described in the section 2.5 and characterized by the parameters listed in the Table 1. The boundary conditions (see section 2.1, step 7) used to select the more loaded beams (oriented along the *X* axis) consisted of an overall deformation $\langle\varepsilon\rangle = [\langle\varepsilon_x\rangle \dots 0]$, with $\langle\varepsilon_x\rangle$ being the strain component along the *X* axis set to 10^{-4} for the sake of simplicity. The algorithm, once introduced the experimental mechanical properties and calculated the elastic solution (see section 2.1, step 8), selected the beams that were directed according to the internal stress by deleting the least stressed beams while maintaining structural continuity (see section 2.1, steps 9 - 11). At the end of the routine completed by the orientation of the beams (see section 2.1, steps 10 and 11), the algorithm, on the basis of the pseudocode listed in Section 2.1, introduced a parametric curvature to each beam and, at the same time, resized the beams (varying the circular cross section) to achieve the desired porosity (see section 2.1, step 12). Figure 5 shows the effect of the algorithm elaboration on the cubic RVE (a, b and c) and the 3D printed polymeric specimen (d).

At the end, (see section 2.1, steps 13 and 14) two physical models characterized by the morphometric parameters listed in table 1 were realized by rapid prototyping technique with the purpose of subjecting them to compression test; the three homogenized Young's moduli have been evaluated in the three mutually perpendicular directions *X*, *Y* and *Z* of the two cubic specimens. Once built the two virtual RVEs described in section 3, boundary conditions,

approximating the compression tests, have been applied in Ansys environment, assuming absence of sliding of the zones in contact with the rigid bases characterizing the polymeric specimen. Then the three Young's moduli have been evaluated in the three directions *X*, *Y* and *Z* of the cubic RVE.

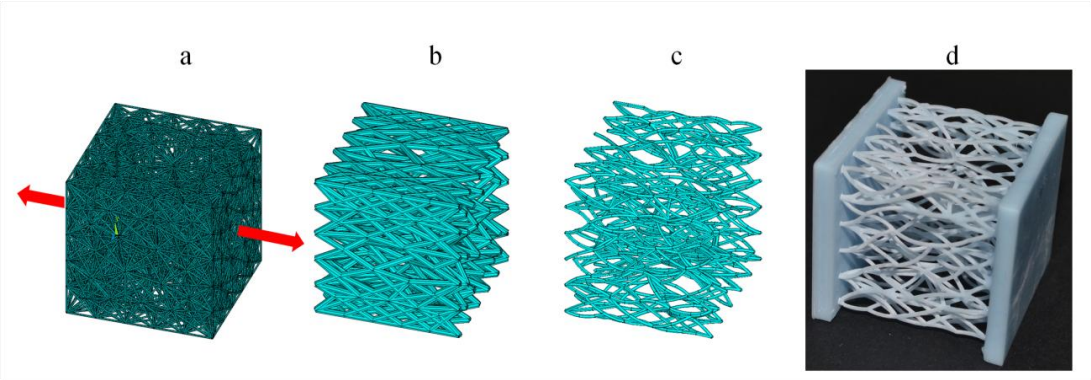

Figure 5. Effect of the algorithm elaboration on the cubic RVE: a) isotropic cubic lattice structure showing the direction of the imposed displacements (*X* axis); b) cubic lattice structure showing resized beams oriented along the *X* axis; c) cubic lattice structure showing curved beams; d) 3D printed polymeric specimen.

5. Results

5.1 Beam sorting criteria results

The choice of beam sorting criteria was based on a comparison of the FEM simulation results of the final cubic RVE showing the beams oriented along the *X* axis. For the sake of simplicity, an input Young's modulus for beams equal to $E_i = 1Pa$ and with an overall deformation $\langle \varepsilon_x \rangle = 10^{-4}$ were introduced as input parameters. The results used for comparison were maximum values (*Maxv*) recorded in the whole RVE for von Mises equivalent stress, principal stress (absolute value), and shear stress (absolute value). To understand the average behaviour of the RVE structure and to avoid the possibility that abnormal maximum values could affect the evaluation, it was also considered the arithmetic mean value (*Amv*) of the maximum values recorded in each beam of the same items that was calculated by the following formula:

$$Amv = \frac{1}{n}\sum_{i=1}^{n} X_{Max,i} \quad (7)$$

with *n* being the number of beams and $X_{Max,i}$ representing, alternately, the maximum values of von Mises equivalent stress, principal stress (absolute value) and shear stress (absolute value) in the i-th beam.

Finally, a comparison was also made between the homogenized Young's moduli of the RVE, calculated in the preferred direction of the beams (*X*-axis) using the three different criteria. Table 2 show the used criteria and the comparison among them.

Table 2 Comparison of the criteria.

CRITERIA / OUTPUT	Elastic strain Energy		$\sigma_{eq\ (Von\ Mises)}$		$\sigma_{principal,\ Max}$	
	Maxv	*Amv*	*Maxv*	*Amv*	*Maxv*	*Amv*
$\sigma_{eq,\ (Von\ Mises)}$ [Pa]	3.2032E-04	1.2202E-04	3.1591E-04	9.2860E-05	3.1591E-04	1.3007E-04
Abs($\sigma_{principal,\ Max}$) [Pa]	3.2022E-04	1.1862E-04	3.1568E-04	9.1430E-05	3.1568E-04	1.2867E-04
Abs(τ) [Pa]	5.1530E-05	5.9400E-06	4.7010E-05	7.6400E-06	4.7010E-05	6.1900E-06
RVE Young's Modulus (E_x) [Pa]	1.6522E-01		1.6515E-01		1.6412E-01	

As can be seen in the Table 2, regardless of the criterion used, *Maxv* for $\sigma_{eq,\ (von\ Mises)}$ and Abs ($\sigma_{principal,\ Max}$) assumes about the same value, while *Maxv* for Abs (τ) assumes a value of about one order of magnitude lower. The criterion that sorts/eliminates the beams according to σ_{eq} (von Mises) allows to have in output a high homogenized Young's modulus value for the RVE, and, at the same time, to register relatively low *Maxv* for $\sigma_{eq,\ (Von\ Mises)}$ and Abs ($\sigma_{principal,\ Max}$) and moreover a low *Maxv* for Abs (τ). Using this criterion, we also have the lowest *Amv* for the same output results, with the exception of shear stresses that, however, remain over one order of magnitude lower compared to normal stresses. From the structural point of view, in the context of small deformations, the target was the optimization of the structural stiffness. Having to choose an internal configuration of the RVE lattice structure, boundary conditions and amount of material (porosity) being equal, the author chose equivalent von Mises stress criterion for subsequent FEM calculations. This criterion gave a beam configuration that showed a high Young's modulus and recorded, inside, the less burdensome stress state.

5.2 FEM results

A photopolymer named RD 096 blue (Digital Impression Resin, produced by DWS srl - Via Lago di Levico, 3 - 36010 Zanè (VI), Italy) was chosen for the 3D printing; this polymer, after UV post-curing, is characterized by the following elastic material properties: E = 3.120GPa and v = 0.3. These properties have been introduced as input parameters in the described algorithm for the linear elastic modelling of the curved beams. In order to take account of the real testing conditions all the degree of freedom of the nodes belonging to the contact plane between specimen and the polymeric bases, have been set equal to zero in order to simulate the constraint effect of the base. The calculation of Young's modulus was carried out by imposing to the free side of the RVE perpendicular to the compression axis, an arbitrary displacement and obtaining its reaction force as the sum of the nodal forces. Initial section ($Lrve^2$) has been considered as reference in the calculation. The results of the simulations, in terms of Young's modulus, conducted on the cubic RVEs are collected in Table 3:

Table 3 FEM results.

	RVE1	RVE2
E_x (MPa)	13.596	1.585
E_y (MPa)	0.122	0.038
E_z (MPa)	0.108	0.034

5.3 Experimental results

The results of the uniaxial compression tests in terms of Young's modulus, conducted on the cubic specimens are collected in Table 4. The reported results are the arithmetic mean value of the five specimens printed for each direction (X, Y and Z):

Table 4 Experimental results.

	RVE1	RVE2
E_x (MPa)	12.334	1.594
E_y (MPa)	0.124	0.038
E_z (MPa)	0.097	0.036

5.4 Comparisons between experimental and FEM results

The histograms reported in Figure 6 shows the comparison of experimental and numerical results in terms of Young's modulus. The percentage relative errors in the calculation of Young's moduli E_x, E_y and E_z of RVE1were respectively equal to: Err_x = -10.22%, Err_y = 1.62%, Err_z = -1.52%; the percentage relative errors in the calculation of Young's moduli E_x, E_y and E_z of RVE2 were respectively equal to: Err_x = 0.55%, Err_y = -0.98%, Err_z = 6.69%.

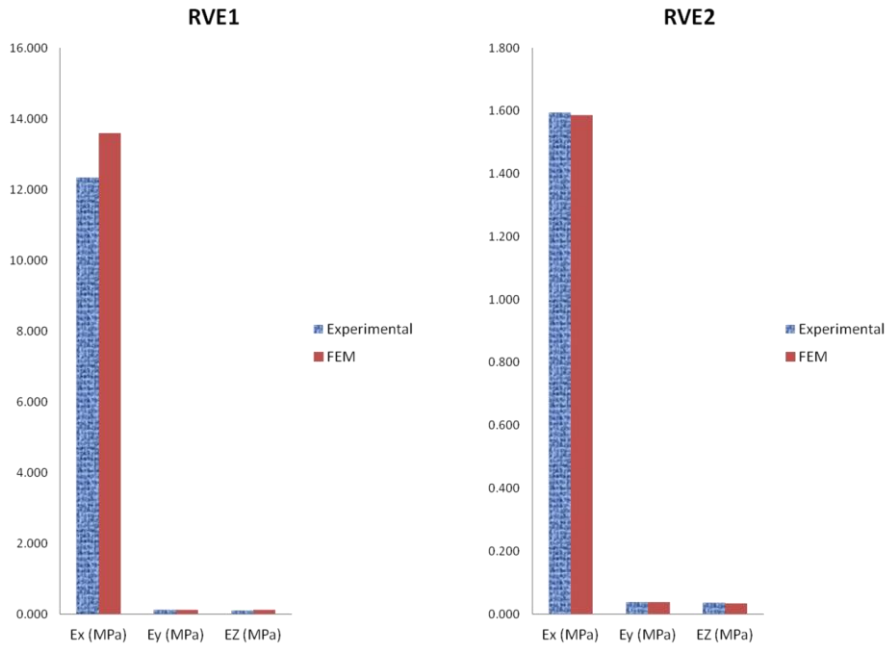

Figure 6. Experimental/numerical correlation in terms of Young's modulus.

6. Discussion, conclusions and perspectives

This work deals with the development, the application and the experimental validation of a procedure based on an original algorithm [16], running in a finite element environment, operating inside a three-dimensional solid of any shape replacing the continuous mass of the solid with an appropriate lattice structure showing curved cylindrical micro-beams, sharing with it border and boundary conditions. The algorithm input parameters are: average minimum distance between convergence nodes, target porosity, target ANB, radius of the SSS, average beam curvature and beams' mechanical properties. At the beginning, the algorithm generates an appropriate isotropic network of randomly oriented beams; then it adapts the network to the loads induced by the boundary conditions according to an appropriate criterion; at the end, a routine introduces a variable curvature at each beam in order to control the homogenized

Young's modulus of the porous structure. To show a practical application of the algorithm and for the validation of the final FEM model characterized by a one-dimensional element (beams) based network, a cubic representative volume element (RVE), properly sized, was chosen to facilitate the analysis of mechanical behaviours. By implementing PBC, the algorithm was able to retrieve the whole stiffness matrix of the cubic RVE. In this way, once properly curved and oriented the beams along a particular direction, the relationship between the compact material Young's modulus in input and the resulting homogenized Young's modulus of the porous RVE, along the main beam direction, was estimated. In this case study, once sized the beams' cross sections according to the desired porosity, the algorithm created two solid CAD models that were converted in .stl files and printed by a 3D printer using an appropriate polymer (the two models differ only in the curvature of the beams). The FEM results were compared with experimental ones obtained by compression tests conducted on the printed cubic RVE. The FEM and experimental results were very close with a mean relative error of 3.60% (see figure 6).The worst correspondence between experimental and predicted elastic modulus has been observed for the sample RVE1 along the *X* axis. A three-dimensional element based network usually gives us results more close to reality. In this case, it would have been possible to build a three-dimensional element based FEM model after the realization of the CAD solid model (see section 2.1, step 13). Such a model would have required a very high computational burden significantly impairing the computing speed that is one of the peculiar characteristics of a parametric variational analysis. However, in this case the closeness between FEM and experimental results confirmed the validity of the "beam element – based" network in terms of Young's modulus. This Experimental/numerical correlation confirms the effectiveness of the procedure in this phase of design characterized by virtual realization of the parametric model, simulations of the elastic mechanical behaviour and three-dimensional printing. Possible applications could be the production of those porous tissues for which it is required a set value of porosity a set external shape, a low weight and heterogeneity of the mechanical properties at the micro and macro levels as for example in the field of research of the CATE for production of scaffolds (bone-like structured foams) and in the field of research of ergonomics for production of highly structured foams. The algorithm, subjected to further validation, could possibly be

applied to other areas of engineering. It can be easily modified in order to be able to control, for example, the average resistant section of the curved beams, or, even better, the resistant section of each beam according to the boundary conditions. Moreover, possible future developments of FEM modelling may be the implementation of new material properties to cover the field of geometrical and material nonlinearity, the evaluation of the effect of large deformations and the analysis of the influence of the mutual contacts among curved beams.

Acknowledgements

We acknowledge the support of Giovanni Marinaccio and Angelo Salamini (Sintesi Sud S.r.l. Corso Vittorio Emanuele, 233 83031 Ariano Irpino (AV), Italy) for the three dimensional printing service, Prof. Loredana Incarnato and Eng. Emilia Garofalo, Ph.D (Department of Industrial Engineering, University of Salerno, Via Giovanni Paolo II, 132, 84084 Fisciano, SA, Italy), for the experimental testing phase.

References

[1] Deaton JD, Grandhi RV. A survey of structural and multidisciplinary continuum topology optimization: post 2000. Struct Multidiscip Optim 2014; 49(1): 1–38

[2] Rozvany GIN. Aims, scope, methods, history and unified terminology of computer-aided topology optimization in structural mechanics. Struct Multidiscipl Optim 2001; 21: 90–108.

[3] Wolff J. The law of bone remodelling. Berlin, Germany: Springer-Verlag, 1986.

[4] Cowin SC. Bone Mechanics Handbook, second ed. USA: CRC Press, 2001.

[5] Fernandes P, Rodrigues H, Jacobs C. A model of bone adaptation using a global optimisation criterion based on the trajectorial theory of Wolff. Comput Methods Biomech Biomed Eng 1999; 2 (2): 125–138.

[6] Garcia JM, Doblaré M, Cegonino J. Bone remodelling simulation: a tool for implant design. Comput Mater Sci 2002; 25: 100–114.

[7] Jacobs CR, Simo JC, Beaupre, GS, Carter, DR. Adaptive bone remodeling incorporating simultaneous density and anisotropy considerations. J Biomech 1997; 30 (6): 603–613.

[8] Cowin SC. Bone stress adaptation models. ASME J Biomech Eng 1993; 115: 528 - 533.

[9] Huiskes R, Hollister SJ. From Structure to process, from organ to cell: recent developments of FE-analysis in orthopaedic biomechanics. ASME J Biomech Eng 1993; 115: 520–527.

[10] Coelho PG, Fernandes PR, Rodrigues HC, Cardoso JB, Guedes JM. Numerical modeling of bone tissue adaptation – a hierarchical approach for bone apparent density and trabecular structure. J Biomech 2009; 42 (7): 830–837.

[11] Hambli R, Katerchi H, Benhamou CL. Multiscale methodology for bone remodelling simulation using coupled finite element and neural network computation. Biomech Model Mechanobiol 2011; 10: 133–145.

[12] Tsubota K, Suzuki Y, Yamada T, Hojo M, Makinouchi A, Adachi T. Computer simulation of trabecular remodelling in human proximal femur using large-scale voxel FE models: approach to understanding Wolff's law. J Biomech 2009; 8: 1088–1094.

[13] Luo ZP, An KN. A theoretical model to predict distribution of the fabric tensor and apparent density in cancellous bone. J Math Biol 1998; 36 (6): 557–568.

[14] Boyle C, Kim IY. Three-dimensional micro-level computational study of Wolff's law via trabecular bone remodelling in the human proximal femur using design space topology optimization. J Biomech 2011; 44 (5): 935–942.

[15] Baldino l, Naddeo F, Cardea S, Naddeo A, Reverchon E. FEM modeling of the reinforcement mechanism of Hydroxyapatite in PLLA scaffolds produced by supercritical drying, for Tissue Engineering applications. J Mech Behav Biomed Mater 2015; 51: 225–236.

[16] Naddeo F. 2016 Metodologia per la realizzazione ottimizzata rispetto ai carichi di scaffold tissutali, Patent 102016000047650.

[17] Naddeo F, Baldino L, Cardea S, Naddeo A, Reverchon E. Optimization of an ad hoc realized lattice structure structured RVE for FEM modeling of nanoporous biopolymeric scaffolds obtained by supercritical fluids assisted process. Chem Eng Trans 2016; 49: 169-174.

[18] Lakatos É, Bojtár I. Trabecular bone adaptation in a finite element frame model using load dependent fabric tensors. Mech Mater 2012; 44: 130–138.

[19] Ma HS, Pre´vost, JH, Scherer GW. Elasticity of DLCA model gels with loops. Int J Solids Struct 2002; 39: 4605–4614.

[20] Rainer A, Giannitelli SM, Accoto D, Porcellinis S, Guglielmelli E, Trombetta M. Load-Adaptive Scaffold Architecturing: A Bioinspired Approach to the Design of Porous Additively

Manufactured Scaffolds with Optimized Mechanical Properties. Ann Biomed Eng 2012; 40(4): 966-75.

[21] Hori M, Nemat-Nasser S. On two micromechanics theories for determining micro - macro relations in heterogeneous solids. Mech Mater 1999; 31: 667–682.

[22] Cricrì G, Garofalo E, Naddeo F, Incarnato L. Stiffness constants prediction of nanocomposites using a periodic 3D-FEM model. J Polym Sci Part B Polym Phys 2012; 50: 207–220.

[23] Naddeo F, Cappetti N, Naddeo A. Automatic versatile parametric procedure for a complete FEM structural analysis of composites having cylinder-shaped reinforcing fibres. Comput Mater Sci 2014; 81: 239–245.

[24] Pothuaud L, van Rietbergen B, Charlot C, Ozhinsky E, Majumdar S. A new computational efficient approach for trabecular bone analysis using beam models generated with skeletonized graph technique. Comput Methods Biomech Biomed Eng 2004; 7 (4): 205–213.

[25] van Lenthe GH, Stauber M, Müller R. Specimen-specific beam models for fast and accurate prediction of human trabecular bone mechanical properties. Bone 2006; 39: 1182–1189.

[26] Pirard R, Pirard J-P. Aerogel compression theoretical analysis. J Non-Cryst Solids 1997; 212: 262-267.

[27] Cappetti N, Naddeo A, Naddeo F, Solitro GF. Finite elements/Taguchi method based procedure for the identification of the geometrical parameters significantly affecting the biomechanical behavior of a lumbar disc. Comput Methods Biomech Biomed Engin 2016; 19(12): 1278-1285.

Figure Captions

Figure 1. Algorithm fundamental steps for elaborating a generic cubic solid mass withstanding generic boundary conditions: A) step 1; B) step 2; C) steps 3 and 4; D) step 5 ; E) steps 6 - 11; F) steps 12 - 13; G) 3D printed polymeric specimen.

Figure 2. Example of an initial isotropic cubic RVE. For readability purposes, fewer mesh wires than those used in the calculation are represented.

Figure 3. Percentage ratio of E_x *and* E_y to E, in function of the beams' curvature represented by "*d/dist*", the porosity P being constant; E_z has not been introduced in the graph since it is quite superimposable to E_y one.

Figure 4. Printed specimens: in the first row, the three configurations of the RVE1 specimen are shown; in the second row, the three configurations of the RVE2 specimen are shown.

Figure 5. Effect of the algorithm elaboration on the cubic RVE: a) isotropic cubic lattice structure showing the direction of the imposed displacements (X axis); b) cubic lattice structure showing resized beams oriented along the X axis; c) cubic lattice structure showing curved beams; d) 3D printed polymeric specimen.

Figure 6. Experimental/numerical correlation in terms of Young's modulus.

Tables

Table 1 Morphometric input parameters characterizing the two cubic RVEs to be printed.

	RVE1	**RVE2**
Lrve	2cm	2cm
dist	Lrve/5	Lrve/5
SSS radius	dist*1.75	dist*1.75
Porosity	0.95	0.95
d/dist	0.1	0.25
ANB	4	4

Table 2 Comparison of the criteria.

CRITERIA / OUTPUT	Elastic strain Energy		$\sigma_{eq\ (Von\ Mises)}$		$\sigma_{principal,\ Max}$	
	Maxv	*Amv*	*Maxv*	*Amv*	*Maxv*	*Amv*
$\sigma_{eq,\ (Von\ Mises)}$ [Pa]	3.2032E-04	1.2202E-04	3.1591E-04	9.2860E-05	3.1591E-04	1.3007E-04
Abs($\sigma_{principal,\ Max}$) [Pa]	3.2022E-04	1.1862E-04	3.1568E-04	9.1430E-05	3.1568E-04	1.2867E-04
Abs(τ) [Pa]	5.1530E-05	5.9400E-06	4.7010E-05	7.6400E-06	4.7010E-05	6.1900E-06
RVE Young's Modulus (E_x) [Pa]	1.6522E-01		1.6515E-01		1.6412E-01	

Table 3 FEM results.

	RVE1	RVE2
E_x (MPa)	13.596	1.585
E_y (MPa)	0.122	0.038
E_z (MPa)	0.108	0.034

Table 4 Experimental results.

	RVE1	RVE2
E_x (MPa)	12.334	1.594
E_y (MPa)	0.124	0.038
E_z (MPa)	0.097	0.036

Tables

Table 1 Morphometric input parameters characterizing the two cubic RVEs to be printed.

	RVE1	**RVE2**
Lrve	2cm	2cm
dist	Lrve/5	Lrve/5
SSS radius	dist*1.75	dist*1.75
Porosity	0.95	0.95
d/dist	0.1	0.25
ANB	4	4

Table 2 Comparison of the criteria.

CRITERIA / OUTPUT	Elastic strain Energy		$\sigma_{eq\ (Von\ Mises)}$		$\sigma_{principal,\ Max}$	
	Maxv	*Amv*	*Maxv*	*Amv*	*Maxv*	*Amv*
$\sigma_{eq,\ (Von\ Mises)}$ [Pa]	3.2032E-04	1.2202E-04	3.1591E-04	9.2860E-05	3.1591E-04	1.3007E-04
Abs($\sigma_{principal,\ Max}$) [Pa]	3.2022E-04	1.1862E-04	3.1568E-04	9.1430E-05	3.1568E-04	1.2867E-04
Abs(τ) [Pa]	5.1530E-05	5.9400E-06	4.7010E-05	7.6400E-06	4.7010E-05	6.1900E-06
RVE Young's Modulus (E_x) [Pa]	1.6522E-01		1.6515E-01		1.6412E-01	

Table 3 FEM results.

	RVE1	RVE2
E_x (MPa)	13.596	1.585
E_y (MPa)	0.122	0.038
E_z (MPa)	0.108	0.034

Table 4 Experimental results.

	RVE1	RVE2
E_x (MPa)	12.334	1.594
E_y (MPa)	0.124	0.038
E_z (MPa)	0.097	0.036

Figure 1

Click here to download high resolution image

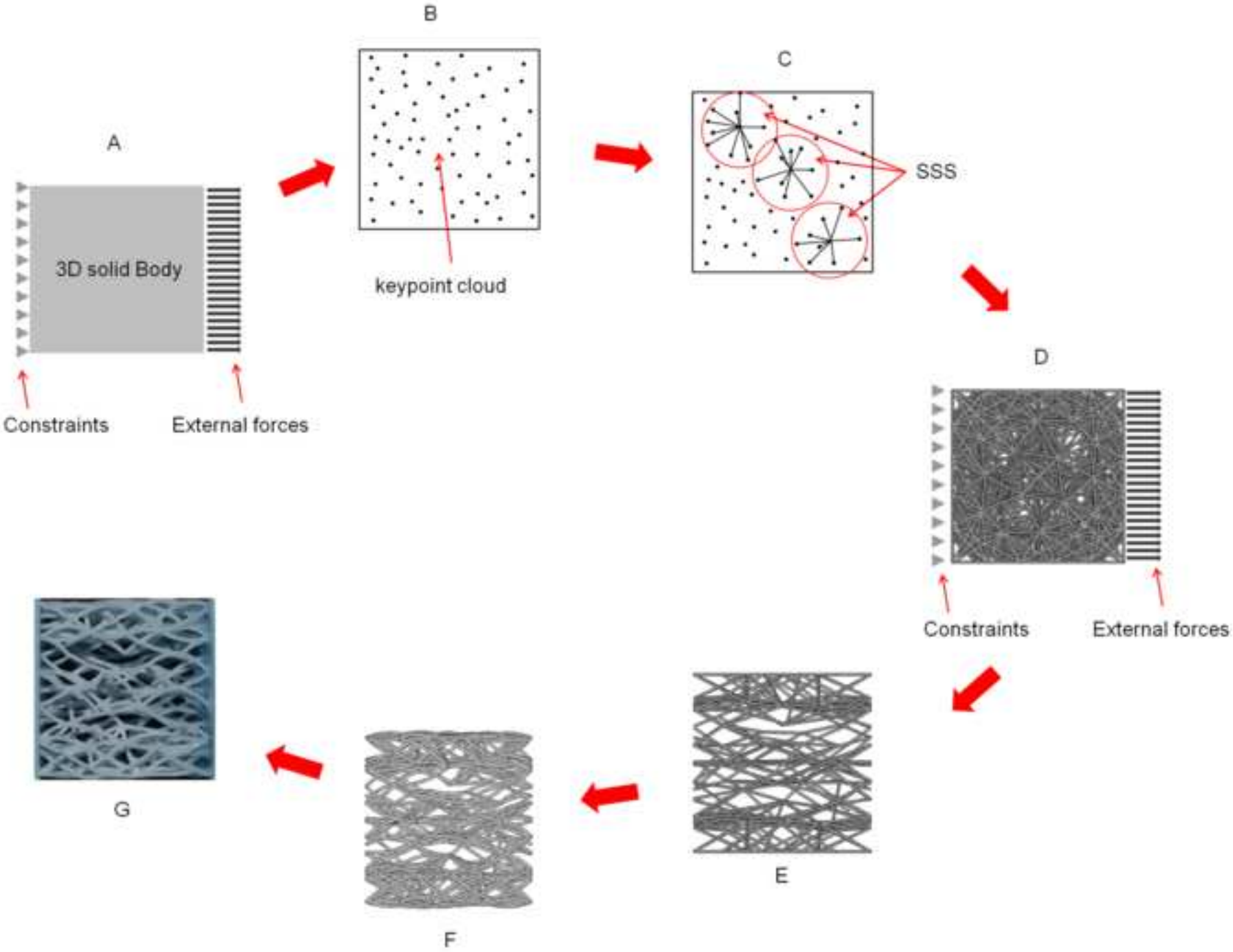

Figure 2

Click here to download high resolution image

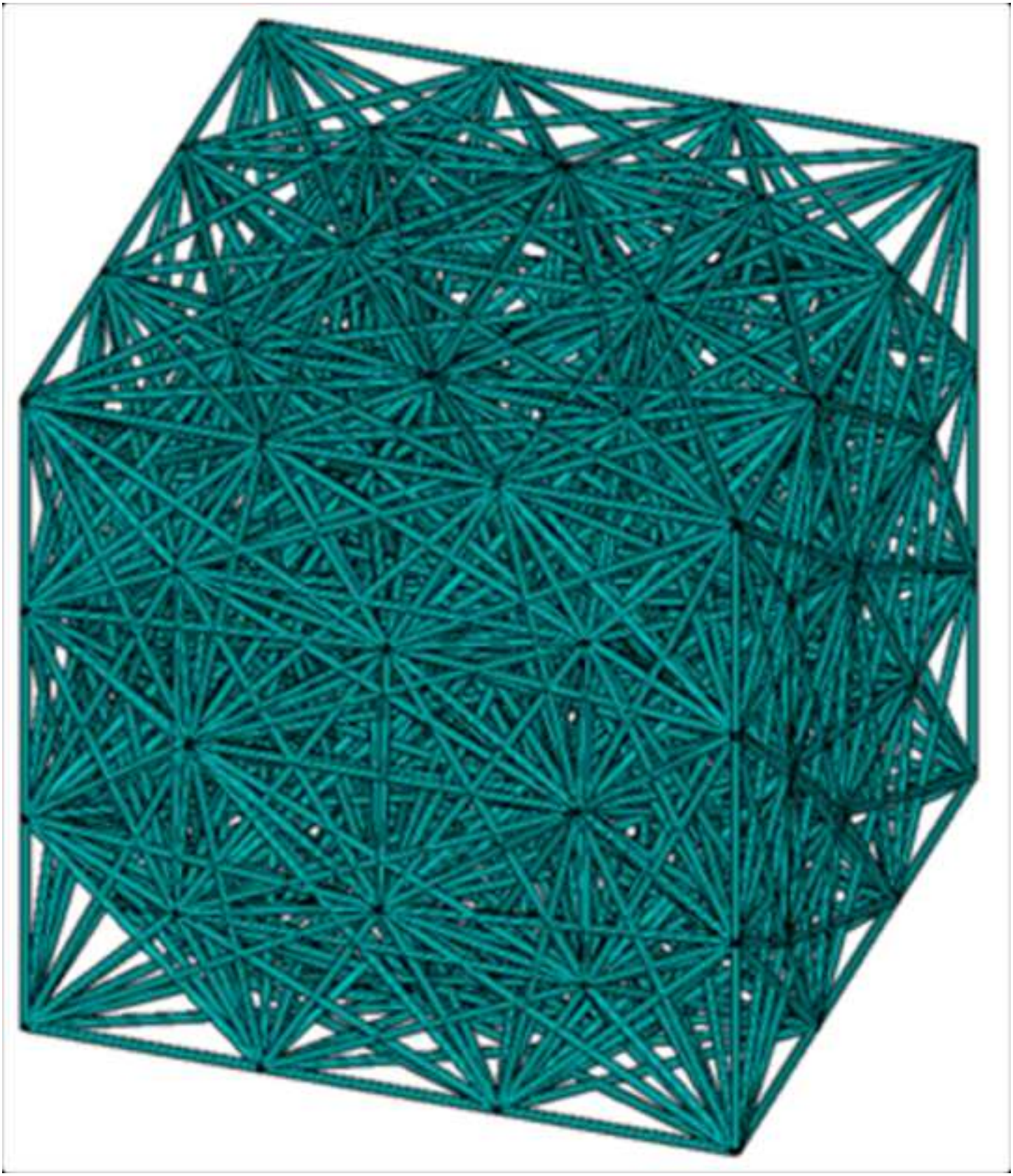

Figure 3

Click here to download high resolution image

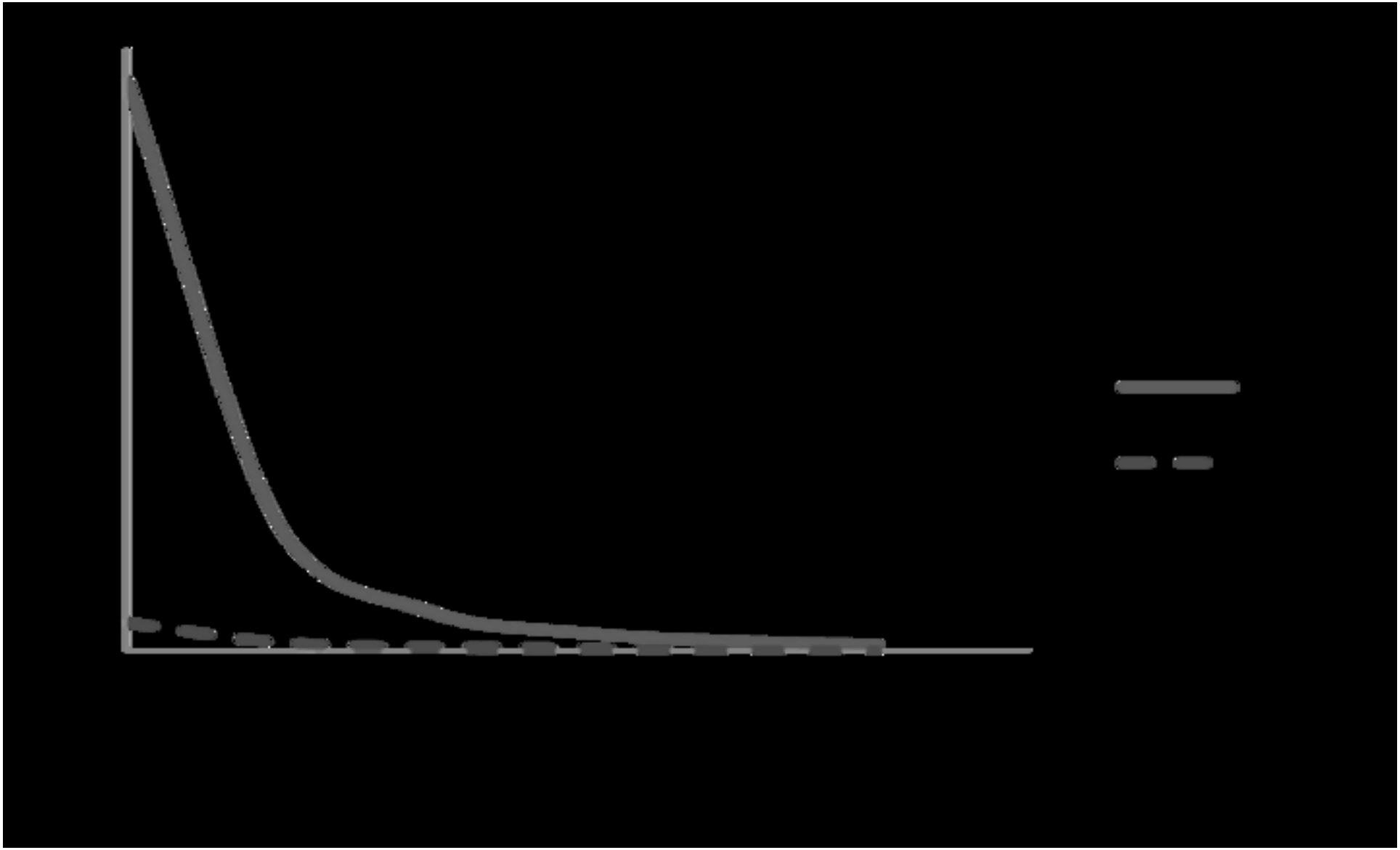

Figure 4

Click here to download high resolution image

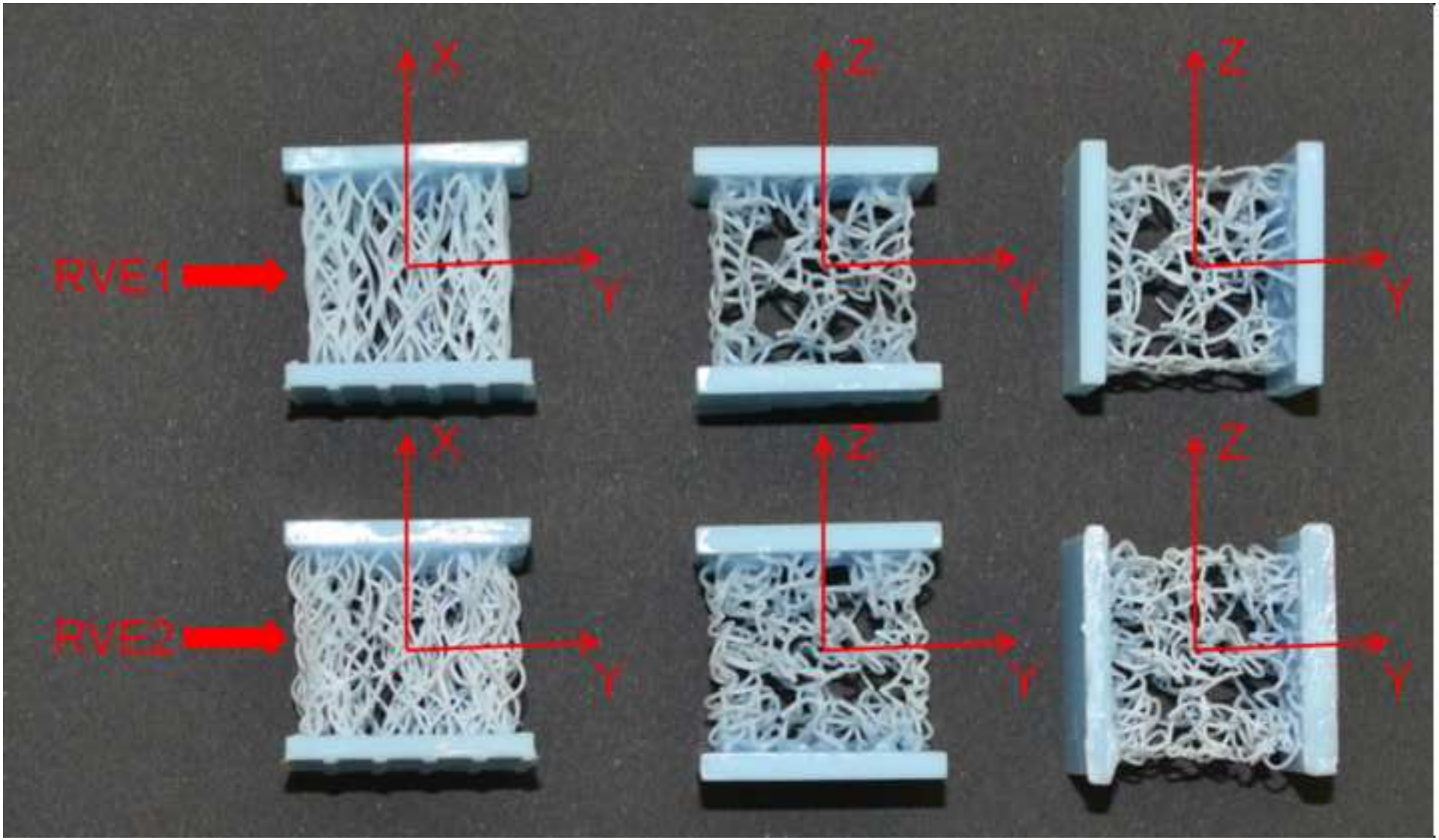

Figure 5

Click here to download high resolution image

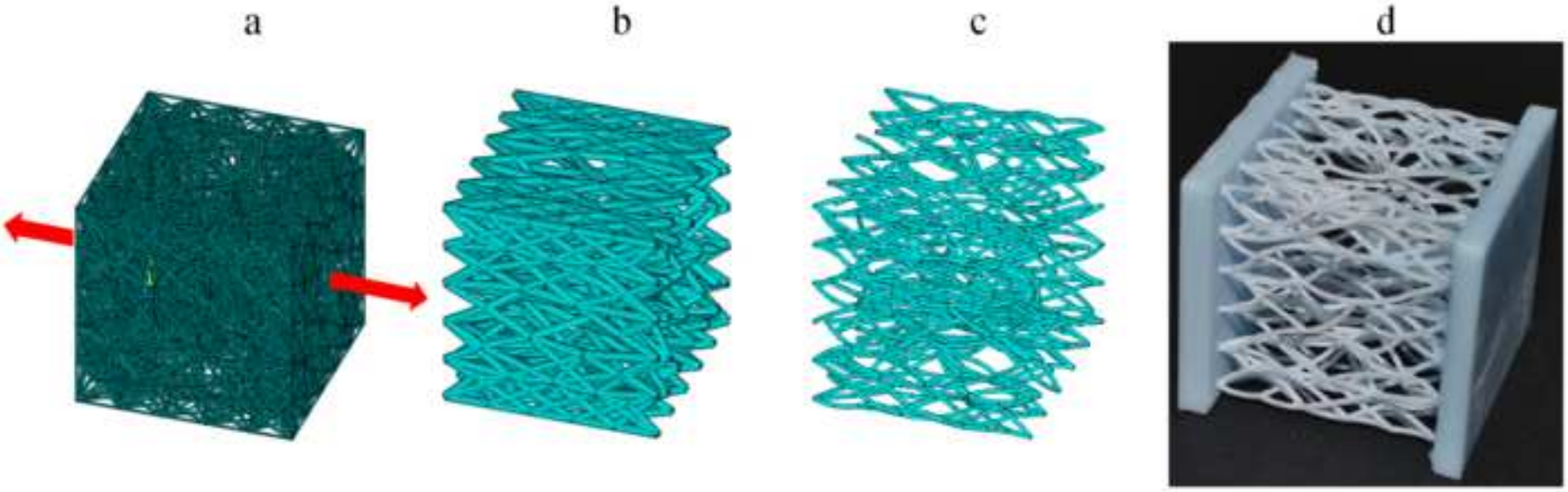

Figure 6

Click here to download high resolution image